Carrier-to-Interference Ratio Measurement Using Moments or Histograms

Yu T. Su, *Member, IEEE,* and Ju-Ya Chen

***Abstract*—Cochannel interference is often the predominant factor that limits the capacity of a cellular mobile radio system. Power control is thus needed so that carrier-to-cochannel interference ratio (CIR) can be maintained within a tolerable bound. Many power control algorithms that require real-time CIR measurement have been proposed but there is very few mentioning of the measurement method. This paper presents viable solutions for real-time CIR estimations under various channel conditions. These solutions are based on either the method of moments or the histogram matching concept. We provide numerical results to demonstrate the usefulness and to compare the performance of the proposed algorithms. It is found that the histogram matching method with a properly-designed nonuniform quantizer offers excellent CIR estimation.**

***Index Terms*—Cochannel interference, MAP estimation.**

I. Introduction

THE ULTIMATE concern of a communication system designer is the quality of the demodulated baseband signals. When cochannel or interchannel interference is present, carrier-to-interference ratio (CIR) or signal-to-interference ratio (SIR) is an important receiver parameter that characterizes the degree of system performance deterioration. For angle-modulated analog waveforms, Prabhu and Enloe [1] derived upper and lower bounds of the minimum baseband SIR over the signaling band in a multiple-interferer environment. These baseband SIR bounds depend on the number of interferers and the radio frequency band CIR. Recently, Mizuno and Shimbo [2] presented an exact analysis of an FM discriminator when the received carrier is modulated by a Gaussian baseband signal. Both thermal noise and a cochannel interferer are considered. The autocorrelation of the signal, interference and noise components, and the cross correlations among them are derived. The relationship between RF band CIR and baseband SIR can be found in [1] and [2]. Other investigations (e.g., [3]) show that CIR is also a good indicator for the quality of digital communication signals.

When a frequency reuse scheme is employed in a cellular mobile communication system to enhance the system's spectral utilization efficiency, a received signal inevitably suffers from interference from other cochannel users. The signal quality requirement of such a cellular system is often specified by a CIR threshold called the protection ratio. For an FDMA system, the cochannel reuse distance, i.e., the minimum distance between two cochannel users and therefore the cell size has to be such that the average CIR is greater than or equal to this minimum required threshold value. Therefore, the system capacity is limited by the multiplicity of the simultaneous usage of the same channel. Furthermore, power control is necessary to reduce cochannel interference and allow as many cochannel users as possible while each maintaining an acceptable CIR. Besides power control [4], we have also seen CIR-based criteria for diversity reception, handoffs, and channel allocation; see references in [6]–[10]. All of these algorithms assume that real-time CIR measurement is available without mentioning how it is obtained.

Kozono [5] used statistical properties of the received waveform's envelope and applied the method of moments to estimate the CIR of a phase-modulated carrier that is corrupted by a single interferer. However, this method is based on a noiseless assumption. The estimated CIR becomes less reliable whenever the operation scenario is different from the assumed one. As CIR is often difficult to measure, Brandão *et al.* [6] introduced a parameter called signal-to-variation power ratio (SVR), and showed it lies between upper and lower bounds of the true CIR for MPSK signals. As SVR is a function of the autocorrelation function of the received samples taken at the symbol rate, it can easily be estimated based on the method of moments. The same SVR idea was later extended to the measurement of signal-to-interference-plus-noise ratio (SINR) of DECT signals [7]. However, in both cases the resulting estimates exhibit a certain degree of bias. Interference projection (IP) and signal projection (SP) methods that project the received baseband samples into the range space or null space formed by the training (or desired) signal were used [8], [9] to estimate SINR of time-division multiple-access signals. Both methods need to know the channel memory length and require a training sequence. The associated estimates need about one second to render an average error of 1 dB. Applying a signal subspace method to the sample covariance matrix of the received narrow-band signal, [10] develops a general SINR estimation algorithm. It requires no channel information but has to perform eigenvector decomposition of the sample covariance matrix.

In the following section, Kozono's method is briefly reviewed. We then extend Kozono's work to other practical situations, suggesting solutions when 1) thermal noise is present; 2) the transmitted signal suffers from Rayleigh fading; and 3) there are more than one interferer. Section III presents a new class of CIR measurement methods that can used in both analog

Paper approved by R. A. Valenzuela, the Editor for Transmission Systems of the IEEE Communications Society. Manuscript received November 15, 1998; revised December 20, 1999. This paper was presented in part at IEEE PIMRC'97, Helsinki, Finland, September 1–4, 1997. This work was supported in part by the National Science Council of Taiwan, R.O.C., under Contract NSC-85-2213E-009-013.

The authors are with the Department of Communication Engineering, National Chiao Tung University, Hsinchu 30010, Taiwan.

Publisher Item Identifier S 0090-6778(00)07102-6.

and digital systems. We first explore the histogram matching concept which has been utilized for other applications. Then a CIR estimation algorithm based on histogram matching is proposed. Variations and modifications of this algorithms are discussed. Performance estimations of our algorithms using computer simulations are given in Section IV. The last section contains our conclusions.

II. CIR Estimation Based on Moments

A. Preliminary

Consider a received radio waveform that is composed of the desired signal and L interference signals. The received signal passes through an intermediate frequency (IF) filter and an envelope detector. The envelope detector's output is sampled and then fed into a microcomputer to evaluate the CIR. Hence the channel considered here includes the transmitter filter, radio channel and the receiver filter. To begin with, let us consider a noiseless environment in which the received signal $R(t)$ is given by

$$\begin{aligned} R(t) &= Se^{j[2\pi f_0 t+\phi_S(t)]} + Ie^{j[2\pi f_0 t+\phi_I(t)]} \\ &= y(t)e^{j[2\pi f_0 t+\psi(t)]} \end{aligned} \tag{1}$$

where f_0 is the cochannel frequency, S and I are the amplitudes of the desired signal and the interferer, respectively; $\phi_S(t)$ and $\phi_I(t)$ are the corresponding modulation waveforms. $y(t)$ and $\psi(t)$ are the envelope and phase of $R(t)$

$$y(t) = \{S^2 + I^2 + 2SI\cos[\phi(t)]\}^{1/2} \tag{2}$$

$$\psi(t) = \tan^{-1}\frac{I\sin\phi_I(t) + S\sin\phi_S(t)}{I\cos\phi_I(t) + S\cos\phi_S(t)} \tag{3}$$

with $\phi(t) = \phi_I(t) - \phi_S(t)$. From (2), we have

$$\begin{aligned} &[y^2(t) - y^2(t+\Delta t)]^2 \\ &\quad = 8S^2I^2\{\cos^2[\phi(t)] - \cos[\phi(t)]\cos[\phi(t+\Delta t)]\} \\ &\qquad + 4SI(S^2+I^2)\{\cos[\phi(t)] - \cos[\phi(t+\Delta t)]\}. \end{aligned} \tag{4}$$

If Δt is properly selected so that $E\{\cos[\phi(t)]\cos[\phi(t+\Delta t)]\} \approx 0$, then [5]

$$E\{y^2(t)\} \approx S^2 + I^2 = a_1 \tag{5}$$

$$E\{[y^2(t) - y^2(t+\Delta t)]^2\} \approx 4S^2I^2 = b_1. \tag{6}$$

Since the cochannel interference comes from another distant mobile cell, the amplitude I is usually less than S. Applying the method of moments, a CIR estimator can be obtained by [5]

$$\Gamma_1 = \frac{S^2}{I^2} = \frac{a_1 + \sqrt{a_1^2 - b_1}}{a_1 - \sqrt{a_1^2 - b_1}}. \tag{7}$$

Assuming the envelope output is an ergodic process, we have

$$E\{y^2(t)\} = \overline{y^2(t)} = \frac{1}{N}\sum_{i=1}^{N} y^2(t_i) \tag{8}$$

$$\begin{aligned} E\{[y^2(t) - y^2(t+\Delta t)]^2\} &= \overline{[y^2(t) - y^2(t+\Delta t)]^2} \\ &= \frac{1}{N}\sum_{i=1}^{N}[y^2(t_i) - y^2(t_i+\Delta t)]^2 \end{aligned} \tag{9}$$

where N is the number of samples and the overbar denotes the time average operator. The resulting CIR estimation algorithm will be referred to as Estimator 1 or Kozono's estimator henceforth.

B. AWGN Channels

We next consider an additive white Gaussian noise (AWGN) channel with a noise power level σ^2. Invoking the ergodic assumption, we can easily show that the time averages of $y^2(t)$ and $[y^2(t) - y^2(t+\Delta t)]^2$ are

$$\overline{y^2(t)} = S^2 + I^2 + 2\sigma^2 \tag{10}$$

$$\overline{[y^2(t) - y^2(t+\Delta t)]^2} = 4S^2I^2 + 8\sigma^2(S^2+I^2) + 8\sigma^4. \tag{11}$$

A reliable estimate of the noise level $\hat{\sigma}^2$ can be obtained by measuring a neighboring band which contains neither signal nor interference. Assuming the availability of $\hat{\sigma}^2$, we have the following CIR estimate:

$$\Gamma_2 = \frac{a_2 + \sqrt{a_2^2 - b_2}}{a_2 - \sqrt{a_2^2 - b_2}} \tag{12}$$

where

$$a_2 = \overline{y^2(t)} - 2\hat{\sigma}^2 \tag{13}$$

$$b_2 = \overline{[y^2(t) - y^2(t+\Delta t)]^2} - 8a_2\hat{\sigma}^2 - 8\hat{\sigma}^4. \tag{14}$$

This estimation scheme is referred to as Estimator 2.

C. Rayleigh Fading Channels

In a mobile communication environment where the desired and the interference signals suffer from Rayleigh fading, the received waveform can be expressed as

$$R(t) = v_1(t)Se^{j[2\pi f_0 t+\phi_S(t)]} + v_2(t)Ie^{j[2\pi f_0 t+\phi_I(t)]}. \tag{15}$$

The resultant squared envelope becomes

$$y^2(t) = v_1^2(t)S^2 + v_2^2(t)I^2 + 2v_1(t)v_2(t)SI\cos[\phi(t)] \tag{16}$$

where $v_1(t)$ and $v_2(t)$ are independent Rayleigh processes with $\overline{v_k^2(t)} = 2\sigma_f^2$, $k = 1, 2$. Moreover

$$\begin{aligned} &[y^2(t) - y^2(t+\Delta t)]^2 \\ &\quad = v_1^4(t)S^4 + v_2^4(t)I^4 + 2v_1^2(t)v_2^2(t)S^2I^2 + 4v_1^2(t)v_2^2(t) \\ &\qquad \cdot S^2I^2\cos^2[\phi(t)] + 4v_1(t)v_2(t)SI\cos[\phi(t)][v_1^2(t)S^2 \\ &\qquad + v_2^2(t)I^2] + v_1^4(t+\Delta t)S^4 + v_2^4(t+\Delta t)I^4 + 2v_1^2(t+\Delta t) \\ &\qquad \cdot v_2^2(t+\Delta t)S^2I^2 + 4v_1^2(t+\Delta t)v_2^2(t+\Delta t)S^2I^2 \\ &\qquad \cdot \cos^2[\phi(t+\Delta t)] + 4v_1(t+\Delta t)v_2(t+\Delta t)SI \\ &\qquad \cdot \cos[\phi(t+\Delta t)] \cdot [v_1^2(t+\Delta t)S^2 + v_2^2(t+\Delta t)I^2] \\ &\qquad - 2v_1^2(t)v_1^2(t+\Delta t)S^4 - 2v_1^2(t)v_2^2(t+\Delta t)S^2I^2 \\ &\qquad - 2v_1^2(t+\Delta t)v_2^2(t)S^2I^2 - 2v_2^2(t)v_2^2(t+\Delta t)I^4 \\ &\qquad - 4[v_1^2(t)S^2 + v_2^2(t)I^2(t)]v_1(t+\Delta t)v_2(t+\Delta t)SI \\ &\qquad \cdot \cos[\phi(t)] - 4[v_1^2(t+\Delta t)S^2 + v_2^2(t+\Delta t)I^2]v_1(t)v_2(t)SI \\ &\qquad \cdot \cos[\phi(t)] - 8v_1(t)v_2(t)v_1(t+\Delta t)v_2(t+\Delta t)S^2I^2 \\ &\qquad \cdot \cos[\phi(t)]\cos[\phi(t+\Delta t)]. \end{aligned} \tag{17}$$

If the random phase $\phi(t)$ is independent of $v_1(t)$ and $v_2(t)$ then the autocorrelation of the squared Rayleigh process is given by [11]

$$\overline{v_i^2(t)v_i^2(t+\Delta t)} = 4\sigma_f^2(1+\rho_{\Delta t}^2), \qquad i=1,2 \tag{18}$$

where $\rho_{\Delta t} = J_0(2\pi f_D \Delta t)$, $f_D = v/\lambda$ is the maximum Doppler frequency resulted from a relative velocity v and carrier wavelength λ and $J_0(\cdot)$ is the Bessel function of the first kind of order zero. If Δt is selected appropriately such that $v_1(t) \approx v_1(t+\Delta t)$, $v_2(t) \approx v_2(t+\Delta t)$, and $\overline{\cos[\phi(t)]\cos[\phi(t+\Delta t)]} = 0$, we have the following time averages:

$$\overline{y^2(t)} = 2\sigma_f^2(S^2+I^2) = a_3' \tag{19}$$

$$\overline{[y^2(t)-y^2(t+\Delta t)]^2} = (1-\rho_{\Delta t}^2)A + B = b_3' \tag{20}$$

where

$$\begin{aligned} A &= 8\sigma_f^4(S^4+I^4) \\ B &= 16\sigma_f^4 S^2 I^2. \end{aligned} \tag{21}$$

If $\rho_{\Delta t}$ is known, then we immediately have a CIR estimate

$$\Gamma_3' = \frac{a_3' + \sqrt{\dfrac{1+\delta}{1-\delta}a_3'^2 - \dfrac{1}{1-\delta}b_3'}}{a_3' - \sqrt{\dfrac{1+\delta}{1-\delta}a_3'^2 - \dfrac{1}{1-\delta}b_3'}} \tag{22}$$

where $\delta = 1-\rho_{\Delta t}^2$. Unfortunately, $\rho_{\Delta t}$ is in general not known to the receiver. As S^2I^2 is often much smaller than (S^4+I^4) in a high CIR environment, the first term on the right-hand side of (20) dominates the value of $\overline{[y^2(t)-y^2(t+\Delta t)]^2}$. Furthermore, we notice that as the correlation coefficient $\rho_{\Delta t}$ approaches to zero, $\overline{[y^2(t)-y^2(t+\Delta t)]^2} \approx 2\overline{y^4(t)} = 2\overline{[y^2(t)]^2}$. Equations (19) and (20) are therefore highly dependent and we have to use higher-order moments. On the other hand, if $\rho_{\Delta t} \approx 1$, then $\overline{[y^2(t)-y^2(t+\Delta t)]^2} \approx 16\sigma_f^4 S^2 I^2$ and Kozono's method can be directly applied in this case. Since $\rho_{\Delta t}$ is a decreasing function of Δt for small Δt, $\alpha = (1-\rho_{2\Delta t}^2)/(1-\rho_{\Delta t}^2) > 1$. Let $X = \overline{[y^2(t)-y^2(t+\Delta t)]^2}$, $Y = \overline{[y^2(t)-y^2(t+2\Delta t)]^2}$, and consider the ratio

$$\begin{aligned} \frac{X^2}{Y} &= X - \frac{X}{Y}(Y-X) \\ &= X - \frac{X}{Y}[\rho_{\Delta t}^2 - \rho_{2\Delta t}^2]A \\ &= \left[1 - \left(1+\frac{X}{Y}\right)\rho_{\Delta t}^2 + \frac{X}{Y}\rho_{2\Delta t}^2\right]A + B. \end{aligned} \tag{23}$$

Our computation shows that the magnitude of the coefficients associated with the first term in (23) is usually much smaller than that in (20) especially when CIR is high ($\geq$15 dB). This observation leads to a new estimation algorithm called Estimator 3:

$$\Gamma_3 = \frac{a_3 + \sqrt{a_3^2 - b_3}}{a_3 - \sqrt{a_3^2 - b_3}} \tag{24}$$

where

$$\begin{aligned} a_3 &= \overline{y^2(t)} \\ b_3 &= \frac{\overline{[y^2(t)-y^2(t+\Delta t)]^2}^2}{\overline{[y^2(t)-y^2(t+2\Delta t)]^2}}. \end{aligned}$$

When we take into account the presence of thermal noise and use an approach similar to that leads to Estimator 2, we then obtain the following estimate:

$$\Gamma_4 = \frac{a_4 + \sqrt{a_4^2 - b_4}}{a_4 - \sqrt{a_4^2 - b_4}} \tag{25}$$

a_4 and b_4 are modified accordingly

$$\begin{aligned} a_4 &= \overline{y^2(t)} - 2\hat{\sigma}^2 \\ b_4 &= \frac{\overline{[y^2(t)-y^2(t+\Delta t)]^2}^2}{\overline{[y^2(t)-y^2(t+2\Delta t)]^2}} - 8a_4\hat{\sigma}^2 - 8\hat{\sigma}^4. \end{aligned}$$

D. Multiple Interferer Case

All the CIR estimation algorithms discussed so far assume that only one interferer is present. In the case of multi-interferer, the received waveform can be written as

$$\begin{aligned} R(t) &= Sc^{j[2\pi f_0 t + \phi_S(t)]} + \sum_{i=1}^{L} I_i c^{j[2\pi f_0 t + \phi_{I_i}(t)]} \\ &= y(t)c^{j[2\pi f_0 t + \psi(t)]} \end{aligned} \tag{26}$$

where $y(t)$ and $\psi(t)$ are the envelope and phase of $R(t)$, i.e.,

$$\begin{aligned} y^2(t) &= S^2 + \sum_{i=1}^{L} I_i^2 + 2S\sum_{i=1}^{L} I_i \cos[\phi_S(t) - \phi_{I_i}(t)] \\ &\quad + 2\sum_{\substack{i,\,j=1 \\ i\neq j}}^{L} I_i I_j \cos[\phi_{I_i}(t) - \phi_{I_j}(t)] \end{aligned} \tag{27}$$

$$\psi(t) = \tan^{-1}\left\{\frac{S\sin[\phi_S(t)] + \sum_{i=1}^{L} I_i \sin[\phi_{I_i}(t)]}{S\cos[\phi_S(t)] + \sum_{i=1}^{L} I_i \cos[\phi_{I_i}(t)]}\right\}. \tag{28}$$

Assuming the desired signal and interferers yield independent statistics, we can show that $E[y(t)] = S^2 + \sum_{i=1}^{L} I_i^2$ and $E[y^2(t) - y^2(t+\Delta t)] = 4S^2\left(\sum_{i=1}^{L} I_i^2\right)$, if Δt is chosen appropriately. It is clear that, depending on the operation scenario, the problem of CIR $\left(\triangleq S^2/\sum_{i=1}^{L} I_i^2\right)$ estimation for this case can be solved by one of the solutions proposed before.

III. Estimation Based on Probability Distributions

As is well known, complete statistical information of a random process is embedded in the family of all finite-dimensional joint probability distributions associated with it. We can measure one of these distributions of the received waveform and compare it with some known probability distributions. What we really want to know is not which one is the closest

to the measured distribution but the parameter values associated with the closest distribution. As real-time estimation of higher-order statistics and distribution is time- and computational-consuming, we limit ourselves to the usage of short-term probability distributions for CIR estimation. Note that the method of moments uses moments of the received signal. The first few moments, however, contain only partial information of the associated short-term probability distribution. We also want to remark that the idea of statistic or probability distribution matching is not new [12], [13] but its application to CIR measurement is.

A. AWGN Channels

Let us begin with a look at the received signal in an AWGN channel

$$R(t) = Se^{j[2\pi f_0 t+\phi_S(t)]}+\sum_{i=1}^{L} I_i e^{j[2\pi f_0 t+\phi_{I_i}(t)]}+n(t)e^{j2\pi f_0 t} \tag{29}$$

where $n(t)$ is a stationary complex low-pass Gaussian process with zero mean and variance $2\sigma_n^2$. The probability density function (pdf) of $y(t)$—the envelope of $R(t)$—is given by [14]

$$p_y(y) = \int_0^\infty ytJ_0(yt)J_0(St)\prod_{i=1}^{L} J_0(I_i t)e^{-(\sigma_n^2 t^2/2)}\,dt, \quad y>0. \tag{30}$$

The pdf of the normalized envelope $x(t)$ defined by

$$x^2(t) = \frac{y^2(t)}{S^2+\sum_{i=1}^{L} I_i^2+2\sigma_n^2} \tag{31}$$

assuming that the interferers have the same power at the receiver front-end, is given by

$$p_x(x) = x\left(1+\frac{\Lambda}{\Upsilon}+\Lambda\right)\int_0^\infty te^{-(t/4)^2}J_0\left(\sqrt{(1+\Lambda+\Lambda/\Upsilon)}xt\right) \cdot J_0\left(\sqrt{\Lambda}t\right)J_0^L\left(\sqrt{\frac{\Lambda}{\Upsilon L}}\,t\right)dt \tag{32}$$

where $\Upsilon = S^2/\sum_{i=1}^{L} I_i^2 = \text{CIR}$ and $\Lambda = S^2/2\sigma_n^2 = \text{CNR}$. Fig. 1 depicts $p_x(x)$ as a function of CIR, CNR, and the number of interferers (L). As the pdf of $x(t)$ is a function of these parameters, an accurate pdf estimation will provide good estimations of the related parameters including CIR. These curves also reveal that SINR is not an accurate signal quality indicator for the same SINR with different CIR and CNR combination results in different pdf's.

B. Rayleigh Fading Channels

When the transmitted signal suffers from frequency-nonselective Rayleigh (Rician) fading, the pdf of $x(t)$ is Rayleigh (Rician) distributed and cannot be distinguished from each other. Therefore, we have to look for other marginal distributions of the received signal. One of the candidates is the pdf of the base-band phase. Given the amplitudes of signal and interference, we can write the pdf of received signal's phase θ as [15, eq. (13)]

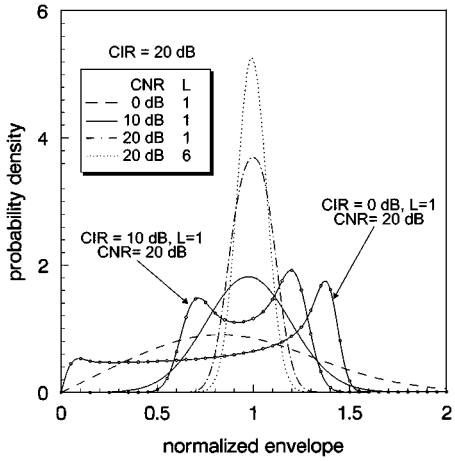

Fig. 1. Pdf's of the normalized envelope.

$$p_\theta(\theta|S,I) = \frac{1}{2\pi}\int_0^\infty \exp\left[-\left(\frac{r^2}{2}+\frac{S^2+I^2}{2\sigma_n^2}-\frac{Sr\cos\theta}{\sigma_n}\right)\right] \cdot I_0\left(\frac{I}{\sigma_n}\sqrt{r^2+\frac{S^2}{\sigma_n^2}-\frac{2Sr}{\sigma_n}\cos\theta}\right)r\,dr \tag{33}$$

where $I_0(\cdot)$ is the zeroth-order modified Bessel function of the first kind. Equation (33) can also be expressed as a function of Λ and Υ

$$p_\theta(\theta|\Lambda,\Upsilon) = \frac{1}{2\pi}\int_0^\infty \exp\left[-\left(\frac{r^2}{2}+\Lambda+\frac{\Lambda}{\Upsilon}-\sqrt{2\Lambda}r\cos\theta\right)\right] \cdot I_0\left[\sqrt{\frac{2\Lambda}{\Upsilon}\left(r^2+2\Lambda-2\sqrt{2\Lambda}r\cos\theta\right)}\right]r\,dr \tag{34}$$

where $\Lambda = S^2/2\sigma_n^2 = \text{CNR}$ and $\Upsilon = S^2/I^2 = \text{CIR}$. If the desired and the interference signals suffer from independent Rayleigh fading with variance equal to $(2-(\pi/2))\sigma_S^2$ and $(2-(\pi/2))\sigma_I^2$, respectively, the pdf of θ becomes

$$p_\theta(\theta) = \int_0^\infty\int_0^\infty p_\theta(\theta|S,I)\,\frac{SI}{\sigma_S^2\sigma_I^2} \cdot \exp\left(-\frac{S^2}{2\sigma_S^2}-\frac{I^2}{2\sigma_I^2}\right)dS\,dI. \tag{35}$$

Equation (35) indicates that $p_\theta(\theta)$ is a function of both CIR and CNR. Shown in Figs. 2 and 3 are $p_\theta(\theta)$ of a 0.3-GMSK modulation signal with carrier frequency 900 MHz transmitted through Jakes' Rayleigh fading channels. It is clear that these pdf's are not only functions of CIR and CNR but also functions of the associated doppler frequency.

C. Maximum a posteriori (MAP) Estimator

Let $Y_i(i=1,2,\cdots,N)$ be the normalized envelope detector output samples of a receiver and $\{R_j, j=1,2,\cdots,M\}$ be a partition of the domain of Y_i, R, i.e., $R=\bigcup_{i=1}^{M} R_i$, $R_i\cap R_j=\emptyset$, if $i\neq j$. The number of the disjoint subsets in the partition M is referred to as the quantization level

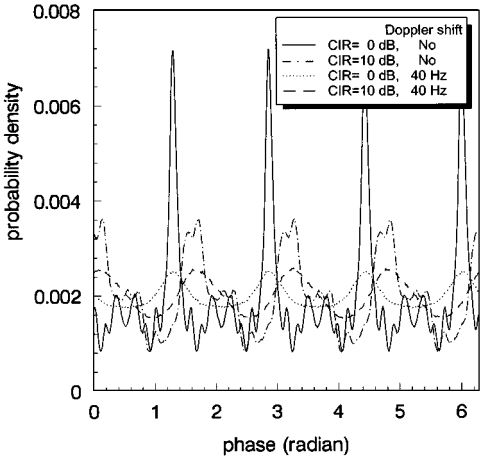

Fig. 2. Pdf's of a GMSK signal's phase with different CIR values.

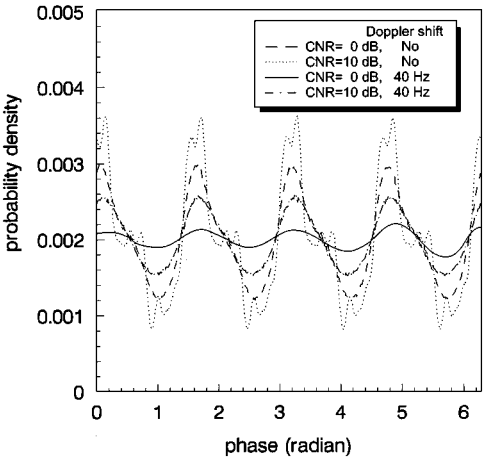

Fig. 3. Pdf's of a GMSK signal's phase with different CNR values.

henceforth. Denote the number of samples fall in the region R_j by q_j and call the ordered pairs $\{(R_j, q_j)\}_{j=1}^{M}$ a histogram. This histogram should converge to the quantized pdf, $\left\{(R_j, p_j)|p_j \triangleq \int_{x\in R_j} p_x(x)\,dx,\ j=1, 2, \cdots, M\right\}$, as $N \longrightarrow \infty$, where $\{p_j\}$ is a candidate quantized pdf or probability mass function (pmf).

Since the quantized pdf is a function of CIR, CNR, and the number of interferers, we can built some priori quantized pdf library models γ_k, $k = 1, 2, \cdots, K$, in terms of the above parameters. The priori library models can be obtained from theory [like (30)], simulation, or field measurements. A CIR estimation can then be derived from matching the measured histogram with the prestored library models. To choose the model γ_k associated with the *a priori* probability $p(\gamma_k)$ that maximizes the *a posteriori* probability $p(\gamma_k|q_1, q_2, \cdots, q_M)$ is equivalent to select a model that satisfies [12], [13]

$$\max_k p(q_1, q_2, \cdots, q_M|\gamma_k)p(\gamma_k). \tag{36}$$

The definition of q_j implies the conditional joint pdf [13]

$$p(q_1, q_2, \cdots, q_M|\gamma_k) = N! \prod_{j=1}^{M} \frac{p_{jk}^{q_j}}{q_j!} \tag{37}$$

where $p_{jk} = \int_{R_j} p_x(x)\,dx$ for model γ_k. After some algebraic manipulations, we can show that (36) is equivalent to [12], [13]

$$\max_k \left[\sum_{j=1}^{M} q_j \log p_{jk} + \log p(\gamma_k)\right]. \tag{38}$$

A number $\hat{k}$ which satisfies (38) implies that the corresponding model $\gamma_{\hat{k}}$ is the MAP model and the associated CIR value is the desired estimation. If the *a priori* distribution $\{p(\gamma_k)\}$ is a uniform one, this MAP test becomes a maximum-likelihood (ML) test. Such a CIR estimation scheme is referred to as MAP (or ML) histogram matching in the subsequent discussions.

D. Least Squares (LS) Estimators

MAP histogram matching results in the smallest decision error if the real model is one of the prestored *priori* library models. From the estimation theory's point of view, the MAP estimate is optimal only if one uses the so-called uniform cost function [16], i.e., the MAP criterion weight all errors equally, no matter how far from the true value an estimate is. On the other hand, the minimum mean-squared estimation error criterion necessitates the evaluation of the conditional mean $E(\mathrm{CIR}|q_1, q_2, \cdots, q_M)$, which is very difficult if not impossible. Intuitively, we would like to select the model that is the closest to measured pmf. There exist several ways to measure the "distance" between two pmf's. Perhaps the simplest one is the Euclidean distance with which we select the model $\hat{\gamma}_k$ that minimizes

$$d_1(\boldsymbol{q}, \boldsymbol{p_k}) = \sum_{j=1}^{M} (q_j - p_{jk})^2 \tag{39}$$

where $\boldsymbol{q}$ and $\boldsymbol{p}_k$ represents the probability distribution $\{q_j\}$ and $\{p_{jk}\}$, respectively. An alternative is the weighted Euclidean distance $\sum_{j=1}^{M} w_j(q_j - p_{jk})^2$. While there are many weighting schemes, the assignment $w_j = p_{jk}^{-1}$ is often used [13]. This weighting then leads to the weighted least squared (WLS) estimator—one that selects the model $\hat{\gamma}_k$ if it minimizes

$$d_2(\boldsymbol{q}, \boldsymbol{p}_k) = \sum_{j=1}^{M} p_{jk}^{-1}(q_j - p_{jk})^2. \tag{40}$$

Note that as the distribution $\{p(\gamma_k)\}$ is not available the MAP histogram matching scheme, (38), is equivalent to an LS estimator which minimizes the distance

$$\begin{aligned} d_0(\boldsymbol{q}, \boldsymbol{p}_k) &= -\sum_{j=1}^{M} q_j \log p_{jk} \\ &= \sum_{j=1}^{M} q_j \log \frac{q_j}{p_{jk}} - \sum_{j=1}^{M} q_j \log q_j \\ &= D(\boldsymbol{q}\|\boldsymbol{p}_k) + H(\boldsymbol{q}) \end{aligned} \tag{41}$$

where $D(\boldsymbol{q}\|\boldsymbol{p_k}) = \sum_{j=1}^{M} q_j \log(q_j/p_{jk})$ is the Kullback Leibler distance between the two pmf's $\{q_j\}$ and $\{p_{jk}\}$ [17] and $H(\boldsymbol{q})$ is the entropy of $\{q_j\}$.

E. Other Design Issues

Other than the choice of the distance measure, there are several design concerns and possible modifications of the generic histogram matching algorithm. The first design concern is the library model size K. For a cellular communication system K can be estimated if one knows the traffic statistics, the user location distribution, the frequency reuse pattern, the cell size and the signal propagation environment. K is also determined by the CIR estimation precision requirement. For a fixed CIR uncertainty range the estimation error can be reduced by increasing the library model size. On the other hand, for a given performance specification, K can be made smaller if the CIR uncertainty range becomes smaller.

The last observation leads to the conclusion that the CIR measurement time can be reduced if we further divide the measurement process into an acquisition mode and a tracking mode. In the acquisition mode, we have to match the measured histogram with all K prestored models. In the tracking mode, we can concentrate our matching effort on those models within a small neighborhood of the previous measurement and thus greatly shorten the search time. Of course this is possible only if we can assume a smooth CIR variation environment. The acquisition time can be further reduced if we divide the acquisition mode into a coarse acquisition phase and a fine acquisition phase. In the first phase, we select $L_1 (\ll K)$ equally-distanced candidate models for initial histogram matching. When the model with the highest matching score is found we then enter the second phase in which L_2 models around the survival model are tested. While the initial phase results in a CIR resolution K/L_1 coarser than the original library the second phase achieves the same resolution. The performance will be the same as that of the single-phase acquisition mode unless we select the wrong model in the initial phase. The probability of such an erroneous selection is usually very small as the distance between two neighboring candidate models in the first phase is large. To make this probability become even smaller we can add another verification phase to check the initial estimate. Furthermore, it is easy to see that the two-phase acquisition process can be extended to an M-phase method in a straightforward manner. The selection of K representatives from the CIR uncertainty region, $\Re$, is worthy of investigation as well. However, since we have no *a priori* information about the distribution of the true CIR value it is more appropriate to apply an uniform partition on $\Re$ so that the distance between two neighboring representative CIR's is a constant.

Another design concern is the choice of the number of the quantization levels M. It is natural to expect the performance to be improved by using a finer partition, or equivalently, a larger M. Given M, we then have to find the optimal partition of R, $\{R_j\}$, which is unlikely to be a uniform one. It makes sense to have finer resolutions on the regions that have higher probability mass. In other words, when building a histogram one should use a nonuniform partition (quantizer) that satisfies the condition $||R_k|| < ||R_l||$ if $p_k > p_l$.

IV. Simulation Results and Discussions

This section provides computer simulation results of the performance of various CIR estimation algorithms and addresses some related design issues. Comparison of the performance of Estimator 2 and the Kozono estimator in AWGN channels is given in Fig. 4. Obviously, the reliability of Estimator 2 depends on the accuracy of the thermal noise power estimator $\hat{\sigma}^2$. The mean estimation performance of Estimator 1 deteriorates as CIR increases while Estimator 2 is always the better of the two unless $\hat{\sigma}^2$ is highly unreliable. But the normalized standard deviation, which is defined by

$$\sigma_e = \frac{\sqrt{E[(\hat{\mathrm{CIR}} - \mathrm{CIR})^2]}}{\mathrm{CIR}} \tag{42}$$

of Estimator 2 is larger than that of Estimator 1. The increase of the estimator variance is due to the introduction of the noise level estimator $\hat{\sigma}^2$ in a_2 and b_2. Equation (14) shows that b_2 is also a function of a_2 while (6) indicates that b_1 is not derived from a_1. The randomness of a_2 increase the variance of b_2 and therefore that of Estimator 2.

Fig. 5 compares the performance of Estimators 1 and 3 in a Rayleigh fading channel. Compared with Estimator 1, Estimator 3 offers amelioration at all but smaller CIR's. When CIR is greater than 3 dB and the Doppler shift is small ($\leq$40 Hz)

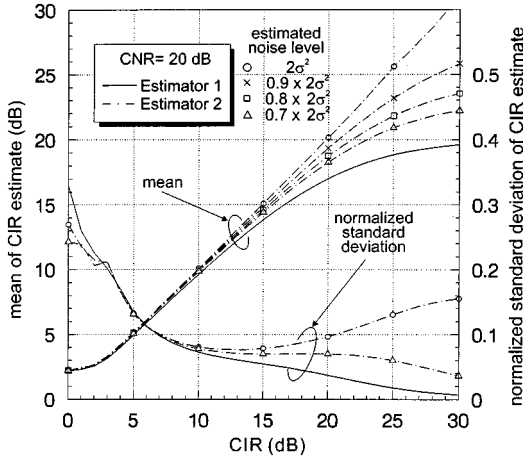

Fig. 4. Effect of the noise level measurement on the performance of CIR estimators in an AWGN channel.

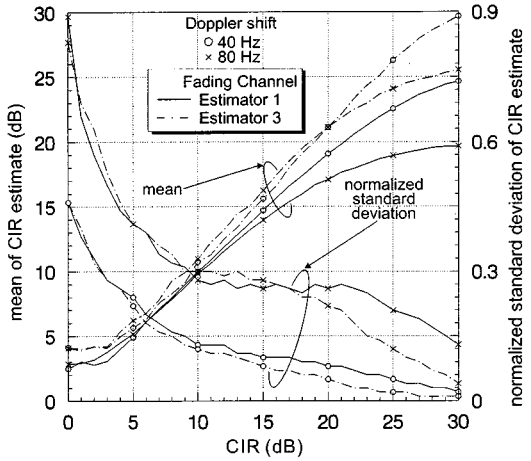

Fig. 5. Comparison of two CIR estimators in a Rayleigh fading channel.

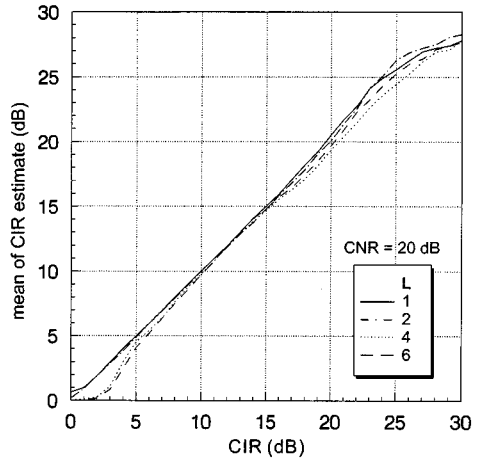

Fig. 6. Performance of the ML histogram matching estimator in a multiple interferer environment.

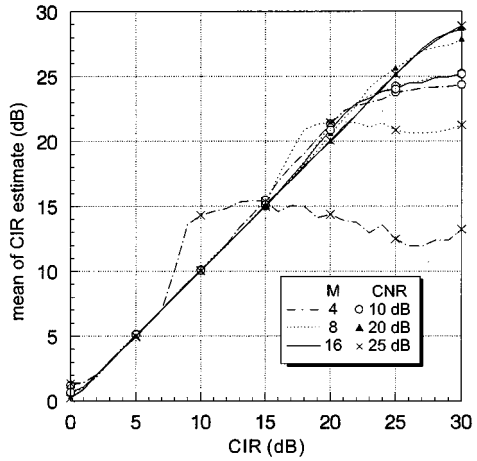

Fig. 7. Influence of the number of quantization intervals on the performance of the ML histogram matching estimator.

Estimator 3 incurs less than 1-dB mean measurement error. Estimator 3 also offers a smaller or at least comparable error standard deviation. In both figures we find that the estimated CIR is biased when the true CIR is small. This is because there is nonzero probability that $a_1^2 - b_1$ in (7) or $a_3^2 - b_3$ in (24) is not positive. Whenever such an event occurs the associated samples have to be discarded as outliers and, as a result, a bias of the CIR estimator is then introduced. If CIR is not too small this probability is negligible but if the interference power is close to the signal power (e.g., 0 dB $<$ CIR $<$ 3 dB), the outlier probability becomes significant enough to make the bias noticeable.

Fig. 6 demonstrates that the histogram matching method can be used effectively in a multiple interferer environment. The estimator is quite robust for most cases of interest. The mean estimation error is always less than 2.5 dB and is less than 1 dB in most cases. Moreover, the histogram matching estimator gives not only the CIR value but also the number of interferers. The effect of the number of quantization levels M is shown in Fig. 7. These curves indicate that M has to be increased to achieve the same performance for a higher CNR. When CNR $\leq$ 20 dB, $M = 4$ or 8 is good enough; increasing M has little or no influence on the performance. But when CNR is 25 dB, $M = 8$ is

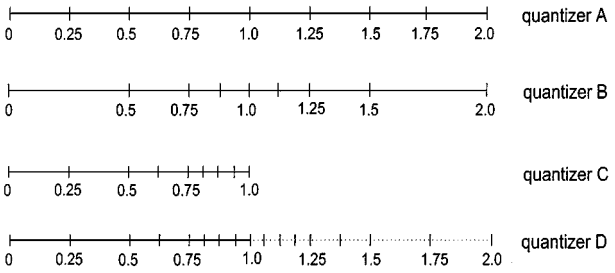

Fig. 8. Four partitions (quantizers) used in the histogram matching estimator.

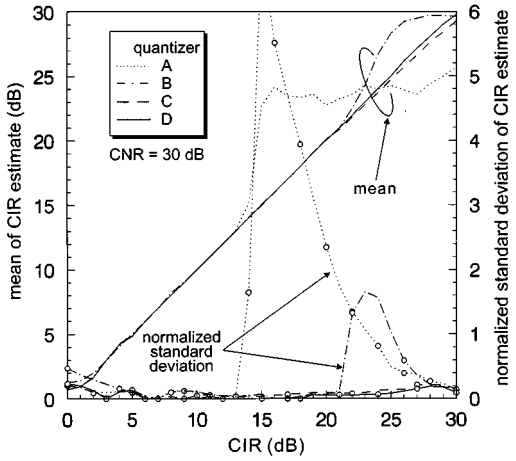

Fig. 9. Effect of partition (quantization) of the normalized envelope range; the ML histogram matching estimator.

not large enough to provide a satisfactory estimation. This is because at high CNR's the probability mass is concentrated around one. Using the same uniform quantizer for all library models we will obtain pmf's that are too close to be distinguishable from each other by the metric d_0.

One way to improve the performance is to increase the number of quantization levels. As mentioned before, nonuniform quantization is another candidate solution. An optimal quantization strategy requires that the quantizer be a function of L, CIR, and CNR. If there are K models in the receiver library we will need the same number of quantizers. Practical consideration suggests that we consider only fixed nonuniform quantizers, i.e., use the same quantizer for all library models.

Fig. 8 shows one uniform quantizer and three nonuniform quantizers, all have eight quantization levels. Taking advantage of the fact that the candidate pdf's are 'almost' symmetric with respect to 1, quantizer C neglects the upper half of the domain R. Quantizer D considers both sides of one but uses the folded histogram for matching. In other words, the histogram value of the $(16 - j + 1)$th interval R_{16-j+1}, q_{16-j+1}, is added to that of the jth interval, $q_j \longleftarrow q_j + q_{16-j+1}$, and only the folded lower half, $(q_1, q_2, \cdots, q_8)$, is used for matching. The performance of these four quantizers are presented in Fig. 9. All three nonuniform quantizers yield smaller mean estimation error magnitude than that of the uniform quantizer. The reduction of the associated standard deviation is even much more impressive. Similar performance improvement, which is not shown because of space limitation, is found when the pdf in (35) is used for histogram matching in Rayleigh fading channels. As Quantizer

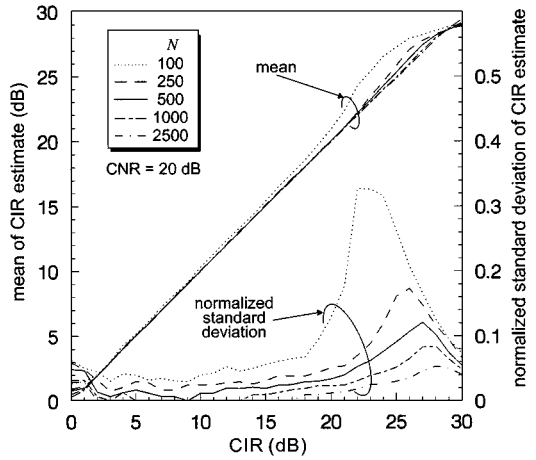

Fig. 10. Effect of the sample size N on the performance of the ML histogram matching scheme.

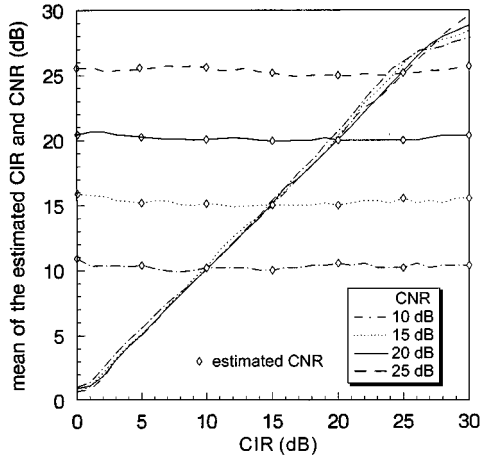

Fig. 12. Simultaneous CIR and CNR estimation using the ML histogram matching.

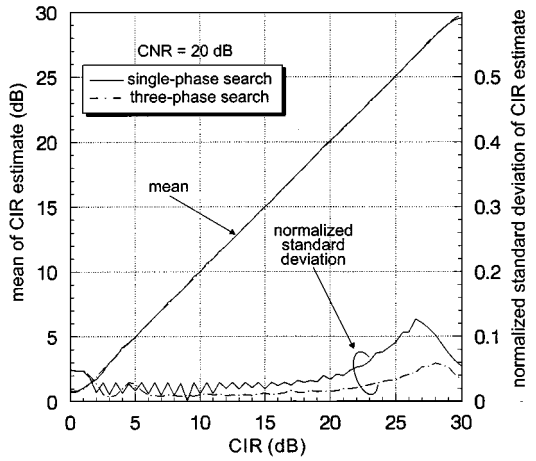

Fig. 11. Performance comparison between single-phase and three-phase search algorithms.

D has the best overall performance it is used for all the following simulations.

In Fig. 10, the effect of the sample size N is evaluated. Although a larger sample size yields a more reliable estimate (smaller mean estimation error and variance) at the cost of larger storage requirement and longer time delay, we find 500 samples is good enough to render reliable CIR estimates. Performance curves for the histogram matching method, unless otherwise specified, are obtained with the same sample size—500, $M = 8$, $K = 31$ and 50 computer runs. With a data rate of 128 kb/s and sampling rate of 1 sample/bit, each estimate requires less than 4 ms.

Compared with the moment method, histogram matching results is more reliable, especially at high CIR's. The bias introduced by the moment method at small CIR's is also eliminated. The CIR estimator resolution is 1 dB. In order to increase the resolution without increasing the computing load, we can apply a multiple-phase acquisition algorithm similar to that described in Section III-E. Performance of a single-phase and a three-phase estimators are depicted in Fig. 11. The single-phase estimator uses 31 models with a resolution of 1 dB while the three-phase estimator has 301 models with a 0.1-dB resolution. The 301 library models are divided into ten groups, each covers a 3-dB range with the middle one as the representative. At the end of the initial phase one of the ten representative models is selected and the second phase then starts testing six models around it, resulting in a resolution of 0.5 dB. The final phase searches the five models round the survival of the second phase, leading to a 0.1-dB resolution. This estimator has to compute the ML distance of (41) for 19 times while the single-phase estimator needs to compute 31 times. The former has a smaller variance in most cases and both estimates yield almost the same mean estimation error. Since the performance curves are depicted with a CIR step size of 0.5 dB, the standard deviations of the single-phase search method, which has a 1-dB resolution, at noninteger CIR points are larger than those at integer CIR points.

We have assumed that perfect CNR information is available so far. CNR can be estimated by the method of moments and a noise power estimator. It can also be derived from ML histogram matching as a pdf is a function of CNR as well. Using histogram matching to estimate both CNR and CIR we have to increase the number of library models though. Fig. 12 depicts some numerical performance examples with 186 prestored library models. Reliable CIR estimation is obtained and CNR estimation error is less than 1 dB for all cases.

Finally, let us examine the influence of the distance measure. Fig. 13 shows that all three distance measures, (39)–(41), render about the same mean estimation error with the WLS distance gives a slightly better performance. The WLS test also has smaller estimator standard deviation in most cases. Another advantage of the WLS test is that, compared with the ML test, it requires less computation. From this and some of previous figures we observe that both the mean estimator error and the normalized estimator standard deviation tends to increase at low or high CIR's. The estimator becomes less reliable at both ends because the "distances" between various priori library models become smaller and in some cases it is so small (on the order of $10^{-5} \sim 10^{-6}$) that they are almost indistinguishable. The largest variance occurs at some high CIR's but not at the highest one (30 dB) since we limit our models to lie between 0–30 dB. The "truncation" makes some large estimation error impossible when

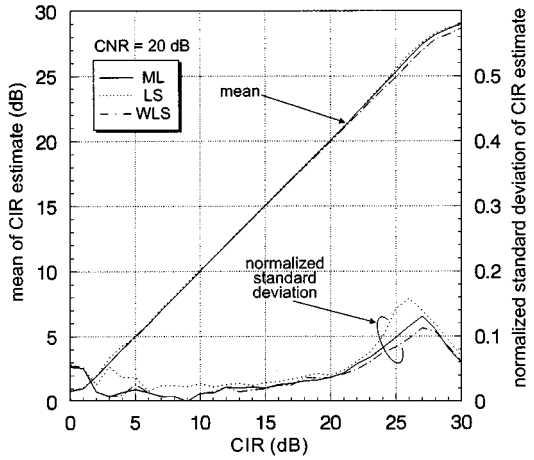

Fig. 13. Influence of the distance measure on CIR estimation.

the true CIR is close to both limits. The reason why the variance does not decrease when the true CIR approaches 0 dB is that the "distance" factor just mentioned dominates the probability of erroneous events. We also have to be reminded of the fact that the standard deviation is normalized by the true CIR value.

V. Conclusions

The necessity of real-time cochannel CIR measurement in a mobile cellular radio network is well known. For analog signals, Kozono had suggested a CIR estimation method that can do without a pilot tone or any other additional supports. His algorithm was derived under the assumption of single interferer and zero thermal noise. When the underlying assumption is not valid, Kozono's algorithm may fail to provide reliable estimates. The first part of this paper presents several new CIR estimation algorithms that can be used in fading and multiple interferer environments. The second part develops CIR estimates using the concept of histogram matching. These estimators can be used in both analog and digital cellular systems. Moreover, they do not need training sequence or eigenvector decomposition and can be performed in either IF band or baseband. Several variations of the direct single-phase histogram matching algorithms are proposed. We can reduce the estimation time by using a multiresolution, multiphase search algorithm and enhance the estimation accuracy by using nonuniformly quantized histogram.

Numerical results demonstrate that the proposed algorithms do outperform Kozono's method and offer reliable CIR estimations within a reasonably small time span (500 samples, or equivalently, less than 10 ms for a data rate greater than 50 kb/s). Of the two classes of algorithms, an algorithm based on histogram matching often result in a better CIR estimate. If the matching metric and the associated quantizer are properly selected, excellent performance can be expected.

References

[1] V. K. Prabhu and L. H. Enloe, "Interchannel interference considerations in angle-modulated systems," *Bell Syst. Tech. J.*, pp. 2333–2358, Sept. 1969.

[2] T. Mizuno and O. Shimbo, "Response of an FM discriminator in the presence of noise and a cochannel interference," *IEEE Trans. Commun.*, vol. 42, pp. 3003–3009, Nov. 1994.

[3] I. Korn, "GMSK with frequency-selective Rayleigh fading and cochannel interference," *IEEE J. Select. Areas Commun.*, vol. 10, pp. 506–515, Apr. 1992.

[4] T.-H. Lee, J.-C. Lin, and Y. T. Su, "Downlink power control algorithms of cellular radio systems," *IEEE Trans. Veh. Technol.*, vol. 44, pp. 89–94, Feb. 1995.

[5] S. Kozono, "Cochannel interference measurement method for mobile communication," *IEEE Trans. Veh. Technol.*, vol. VT-36, pp. 7–13, Feb. 1987.

[6] A. L. Brandão, L. B. Lopes, and D. C. McLernon, "Cochannel interference estimation for M-ary PSK modulated signals," *Wireless Personal Commun.*, vol. 1, pp. 23–32, 1994.

[7] ——, "Quality assessment for pre-detection diversity switching," in *Conf. Rec. IEEE PIMRC'95*, 1995, pp. 577–581.

[8] M. D. Austin and G. L. Stüber, "In-service signal quality estimation for TDMA cellular systems," *Wireless Personal Commun.*, vol. 2, pp. 245–254, 1995.

[9] M. Türkboylari and G. L. Stüber, "An efficient algorithm for estimating the signal-to-interference ratio in TDMA cellular systems," *IEEE Trans. Commun.*, vol. 46, pp. 728–731, June 1998.

[10] M. Andersin, N. B. Mandayam, and R. D. Yates, "Subspace based estimation of the signal to interference ratio for TDMA cellular systems," *Wireless Networks*, vol. 4, pp. 241–247, 1998.

[11] M. J. Gans, "A power-spectral theory of propagation in the mobile-radio environment," *IEEE Trans. Veh. Technol.*, vol. VT-21, pp. 27–38, Feb. 1972.

[12] J. B. Scholz, S. C. Cook, and T. C. Giles, "A scheme for high performance real-time BER measurement," *IEEE Trans. Commun.*, vol. 40, pp. 1574–1576, Oct. 1992.

[13] T. R. C. Read and N. A. C. Cressie, *Goodness-of-Fit Statistics for Discrete Multivariate Data*. New York: Springer-Verlag, 1988.

[14] S. O. Rice, "Probability distributions for noise plus several sine waves—The problem of computation," *IEEE Trans. Commun.*, vol. COM-22, pp. 851–853, June 1974.

[15] A. S. Rosenbaum, "PSK error performance with Gaussian noise and interference," *Bell Syst. Tech. J.*, vol. 48, pp. 413–442, Feb. 1969.

[16] H. L. Van Trees, *Detection, Estimation, and Modulation Theory, Part I*. New York: Wiley, 1968, pp. 55–57.

[17] T. M. Cover and J. A. Thomas, *Elements of Information Theory*. New York: Wiley, 1991.

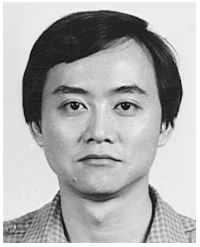

Yu T. Su (S'81–M'83) received the B.S.E.E. degree in 1974 from Tatung Institute of Technology, Taipei, Taiwan, R.O.C., and the Ph.D. degree in electrical engineering from the University of Southern California, Los Angeles, in 1983.

From 1983 to 1989, he was with LinCom Corporation, Los Angeles, where he was involved in the design of various satellite communication systems. Since September 1989, he has been with the Department of Communication Engineering and the Microelectronics and Information Systems Research Center, National Chiao Tung University, Hsinchu, Taiwan. His areas of research interests include communication theory and statistical signal processing.

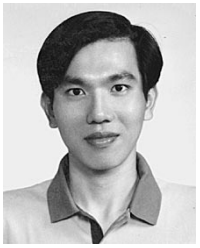

Ju-Ya Chen was born in Kaohsiung, Taiwan, R.O.C., in 1970. He received the B.S., M.S., and Ph.D. degrees in communication engineering from National Chiao Tung University, Hsinchu, Taiwan, in 1992, 1994, and 2000, respectively.

He is currently a System Engineer with the Computer and Communications Laboratories of the Industrial Technical Research Institute. His research interests include detection/estimation theory and spread spectrum communications.

Dr. Chen is a Member of Phi Tau Phi.